Synthesis, spectral and excited state energy transfer studies on new supramolecular ruthenium polypyridyl triads with octakis(methylthio)tetraazaporphyrinzinc(II)

ARTICLE *in* JOURNAL OF MOLECULAR STRUCTURE · MARCH 2009

Impact Factor: 1.6 · DOI: 10.1016/j.molstruc.2008.12.062

Journal of Molecular Structure 921 (2009) 199–207

Contents lists available at ScienceDirect

Journal of Molecular Structure

journal homepage: www.elsevier.com/locate/molstruc

Synthesis, spectral and excited state energy transfer studies on new supramolecular ruthenium polypyridyl triads with octakis(methylthio)tetraazaporphyrinzinc(II)

Rajeev Kumar [a], Rajendra Prasad [a,b,*]

[a] Department of Chemistry, Indian Institute of Technology Roorkee, Roorkee 247667, India
[b] School of Chemical Sciences, Faculty of Science and Technology, The University of the South Pacific, Private MailBag, Laucala Campus, Suva, Fiji

ARTICLE INFO

Article history:
Received 12 September 2008
Received in revised form 22 November 2008
Accepted 19 December 2008
Available online 31 December 2008

Keywords:
Tetraazaporphyrin
Bipyridylruthenium(II)
Phenanthrolineruthenium(II)
Energy transfer
Redox properties
Triads

ABSTRACT

New bichromophoric di- and trinuclear complexes were synthesized through coordinate strapping of one or two $(bpy)_2Ru^{II}$/$(phen)_2Ru^{II}$/$Cp(PPh_3)Ru^{II}$ moieties to [Zn{$(MeS)_8$TAP}] **1**, core. Thus five new complexes of the type [Zn{$(MeS)_8$TAP}{$Ru(bpy)_2$}][PF_6]$_2$ **2**, bent and linear [Zn{$(MeS)_8$TAP}{$Ru(bpy)_2$}{$Ru(phen)_2$}][PF_6]$_4$ **3** and **4**, bent and linear [Zn{$(MeS)_8$TAP}{$Ru(bpy)_2$}{$RuCp(PPh_3)$}][PF_6]$_3$ **5** and **6**, were synthesized and characterized using IR, ^{1}H NMR, UV–visible, and mass spectral data. The trinuclear complexes **3**–**6** possessed bent (κ^4-S^2,S^3,S^7,S^8)[Ru^{II}]$_2$ and linear (κ^4-S^2,S^3,S^{12},S^{13})[Ru^{II}]$_2$ arrangements of the peripheral metallo-chromophore units. Unlike the two reversible reduction waves in complex **1** observed at $E_{1/2}$ −0.34 and −0.60 V, only one reversible reduction wave was observed, between $E_{1/2}$ −0.56 to −0.58 V *vs.* Ag/AgCl, in the di- and trinuclear complexes **2**–**6**. Also in the anodic scans, the dinuclear complexes **2**, as well as linear trinuclear complexes **4** and **6**, exhibited two successive one electron oxidations, the first at $E_{1/2} \sim 0.62$ V due to Ru(II)/Ru(III) process and second at $E_{1/2} \sim 1.16$ V *vs.* Ag/AgCl due to {$(MeS)_8$TAP}/{$(MeS)_8$TAP}$^+$ processes, while the bent trinuclear complexes **3** and **5** exhibited three successive one electron oxidations, i.e. one additional oxidation wave at $E_{1/2}$ 0.88 and 0.90 V *vs.* Ag/AgCl, respectively. In the fluorescence measurements, Soret excitation led to strong [Zn{$(MeS)_8$TAP}] centered S_2 emission together with a rapid intercomponent excitation energy transfer (k 10^7–10^8 s^{-1}) to peripheral Ru(II) unit that showed emission maxima between 535 and 545 nm. Lifetime analysis showed that Ru(II)* emission predominated in the dinuclear complex **2**, but its contribution dropped significantly upon formation of the trinuclear complexes, which has been explained in terms of relative variation of the LUMO energies of the linked chromophores in the excited states.

1. Introduction

In the recent years research on molecule-based nano-devices is getting considerable attention [1] as it offers potentiality to develop ultra small electronic device components to carryout specific roles, through chemical synthesis. Much of this research is focused on development of organic semiconductors for electronic and optoelectronic applications. Several synthetic strategies are being employed to create desired molecular architectures for application in photonic/electronic wires, rectifiers and switches etc. Control of the local environment of functional molecules at individual level and their interactions with other molecular units as well as with the inorganic components are the major objectives that chemists are arduously trying to achieve. Understanding the degree of electronic communication across the supramolecule encompassing its different components is also an area of critical importance that is being actively investigated [2–6].

The transition metals constitute versatile electron reservoirs and sinks in their complexes and hence the supramolecular complexes are the focus of attention, as simple models for design and gaining insight into nature and extent of electronic coupling between different molecular components [7–12]. In this respect the porphyrins and 2,2′-bipyridyl complexes have provided versatile structural platform for building hybrid oligomeric supramolecules and molecular arrays for device applications [13–15]. They possess many useful properties that are desired in the device applications, such as a well defined and rigid molecular framework helpful in separating linked donor–acceptor systems, extended π conjugation, ability to facilitate excitation energy transfer (EET) and electron transfer and high chemical and thermal stability. Thus the di- and oligometallic metallo-porphyrins are considered to be

* Corresponding author. Address: School of Chemical Sciences, Faculty of Science and Technology, The University of the South Pacific, Private MailBag, Laucala Campus, Suva, Fiji. Fax: +679 323 1512.
E-mail addresses: rajenfcy@iitr.ernet.in, prasad_re@usp.ac.fj (R. Prasad).

0022-2860/$ - see front matter © 2008 Elsevier B.V. All rights reserved.
doi:10.1016/j.molstruc.2008.12.062

excellent building blocks in the construction of large multicomponent molecular architectures [16]. The porphyrin–ruthenium(II) hybrid molecular arrays have numerous other potential applications in extremely diverse areas such as in medical diagnosis [17–20], fabrication of data storage devices [21,22], molecular catalysis [23–25], photon funnels, molecular wires, switches, logic gates, rectifiers, circuits, photovoltaic devices and sensor etc. [26–30].

We have recently synthesized several metallo-tetraazaporphyrin complexes with linked polypyridylruthenium(II) moieties [31–34] and have used, some of them in the fabrication of ion selective electrodes for different cations and anions, by incorporating them in liquid polymeric membranes [35–37]. Herein, as an extension of our earlier synthesis works we report synthesis, characterization and photophysical properties of five new supramolecular tetraazaporphyrinzinc(II)-polypyridylruthenium(II) hybrid dyad and triad supramolecules. The geometrical isomeric forms of these molecules make them potential candidates for applications in molecular electronics. As a first step in achieving metallo-tetraazaporphyrin (MTAP) based molecular device components the results reported here are useful in extending application of MTAP's in the development of efficient luminescent sensors for coordinating ions and molecules.

2. Experimental

All common chemicals were of AR grade and were used as received unless otherwise mentioned. Mg foil, $RuCl_3{\cdot}H_2O$, 2,2′-bipyridine, 1,10-phananthroline and LiCl used were obtained from Loba Chemie, India. Tetraethyl ammonium perchlorate, (TEAP) used in cyclic voltammetry studies was obtained from Fluka. Spectroscopic grade CH_2Cl_2 was used for electronic spectral and fluorescence studies. Dry benzene and acetonitrile were used for cyclic voltammetry studies. Benzene was dried over sodium, and the acetonitrile was dried by passing through activated neutral alumina (preheated at 450 °C for 24 h). The precursors [Zn{$(MeS)_8$TAP}] **1**, $[(bpy)_2RuCl_2]{\cdot}2H_2O$, $[(phen)_2RuCl_2]{\cdot}2H_2O$ and $[Cp(PPh_3)_2RuCl]$ were synthesized by the literature methods [38–40].

IR spectra were recorded on a Perkin Elmer – 1600 FTIR spectrophotometer with KBr pellets, electronic spectra on a Shimadzu – 1601 spectrophotometer, in CH_2Cl_2 solutions and fluorescence excitation and emission spectra were recorded on a Fluorolog-3 Horiba Jobin Yvan spectrofluorimeter, in deaerated dichloromethane solutions. The life time measurements were recorded on a Horiba Jobin Yvan-IBH single photon counter and decay curves were analyzed using nonlinear regression method based on the Levenberg–Marquardt (LM) algorithm [41] using Origin 6.0. ^{1}H NMR spectra were recorded on a Bruker Avance 500 MHz Ultrashielded NMR in acetonitrile-d_3 or chloroform-d solutions. The FAB and MALDI-TOF mass spectra (using chloroform solutions) were recorded on Jeol SX-102 and Micromass TofSpec 2E spectrometer, respectively. Voltammetry studies were carried out on a CHI 600A voltammetric analyzer instrument using three-electrode assembly. TEAP (0.1 M) was used as supporting electrolyte. All voltammetric measurements were carried out in the degassed solutions under nitrogen atmosphere. Glassy carbon working microelectrode (0.2 mm dia.), platinum wire auxiliary electrode and Ag/AgCl reference electrodes were used. C, H, N and S analyses were carried out on an Elementar Vario EL III autoanalyser.

2.1. Synthesis of [Zn{$(MeS)_8$TAP}{$Ru(bpy)_2$}][PF_6]$_2$; (**2**)

[Zn{$(MeS)_8$TAP}] **1,** (74.5 mg, 0.1 mmol) and $[(bpy)_2RuCl_2]{\cdot}2H_2O$ (52 mg, 0.1 mmol) in 50 mL benzene–methanol (1:2) mixture were stirred for 18 h followed by heating at reflux for 2 h. The resulting solution was filtered and the volume was reduced to ca. 2 mL by evaporation. To this added a few drops of concentrated solution of NH_4PF_6 in methanol. The solid that precipitated out was collected through filtration and was purified by passage through cellulose column (2.5 × 30 cm), eluting with CH_2Cl_2/petroleum ether (3:1 v/v). *Yield 2:* 103 mg (81%). Λ_M (1.0×10^{-5} M): 144 $\Omega^{-1}cm^2\ mol^{-1}$. IR (KBr): ν 3481b, 1642vs, 1556s, 1413vs, 1335w, 1111w, 841vs, 759w, 649m, cm^{-1}. ^{1}H NMR (CD_3CN): δ 2.8–3.9 (br, 24H, CH_3), 7.1–10.5 (br-m, 16H, Ar-H) ppm. Anal.: calcd. for $C_{44}H_{40}N_{12}S_8P_2F_{12}ZnRu$: C, 36.46; H, 2.76; N, 11.60; S, 17.67%. Found: C, 37.11; H, 2.92; N, 11.16; S, 16.05%.

2.2. Synthesis of [Zn{$(MeS)_8$TAP}{$Ru(bpy)_2$}{$Ru(phen)_2$}][PF_6]$_4$; (**3**) and (**4**)

A mixture of complex **2** (144.8 mg 0.1 mmol) and $[(phen)_2RuCl_2]{\cdot}2H_2O$ (53 mg, 0.1 mmol) in 60 mL dichloromethane/methanol (1:2 v/v) mixture were stirred for 18 h followed by heating at reflux for 2 h. The resultant solution was filtered and volume of the filtrate was reduced to ca. 2 mL by evaporating out the solvent. Addition of a few drops of concentrated methanolic solution of NH_4PF_6 to it precipitated out the mixture of the products. It was filtered and individual isomers were separated by passage through a cellulose column (2.5 × 30 cm) eluting with CH_2Cl_2/petroleum ether (4:1 v/v). *Yield 3:* 78 mg (39%). Λ_M (1.0×10^{-5} M): 410 $\Omega^{-1}cm^2\ mol^{-1}$. IR (KBr): ν 3439b, 1642s, 1552s, 1421vs, 1217w, 1102w, 1029s, 845vs, 755s, 645w, 567m, cm^{-1}. ^{1}H NMR (CD_3CN): δ 2.8–4.5 (br, 24H, CH_3), 6.5–11.0 (br-m, 32H, Ar-H) ppm. Anal.: calcd. for $C_{68}H_{56}N_{16}S_8P_4F_{24}ZnRu_2$: C, 37.10; H, 2.54; N, 10.18; S, 11.64%. Found: C, 37.76; H, 2.51; N, 11.07; S, 10.32%.

Yield 4: 86 mg (43%). Λ_M (1.0×10^{-5} M): 388 $\Omega^{-1}cm^2\ mol^{-1}$. IR (KBr): ν 3448b, 1642s, 1556s, 1421vs, 1307w, 1213w, 1025s, 967s, 845vs, 759s, 718s, 665w, 551 m, cm^{-1}. ^{1}H NMR (CD_3CN): δ 2.9–4.5 (br, 24H, CH_3), 6.7–11.0 (br-m, 32H, Ar-H) ppm. Anal.: calcd. for $C_{68}H_{56}N_{16}S_8P_4F_{24}ZnRu_2$: C, 37.10; H, 2.54; N, 10.18; S, 11.64%. Found: C, 37.36; H, 2.02; N, 11.00; S, 10.76%.

2.3. Synthesis of [Zn{$(MeS)_8$TAP}{$Ru(bpy)_2$}{$CpRu(PPh_3)$}][PF_6]$_3$; (5) and (6)

A mixture of complex **2** (144.8 mg 0.1 mmol) and $[CpRu(PPh_3)_2Cl]$ (72 mg, 0.1 mmol) in 60 mL CH_2Cl_2/methanol (1:2 v/v) mixture were stirred for 18 h followed by heating at reflux for 2 h. The reaction was processed as above. *Yield 5:* 72 mg (33%). Λ_M (1.0×10^{-5} M): 305 $\Omega^{-1}cm^2\ mol^{-1}$. IR (KBr): ν 3444b, 1629vs, 1560s, 1409vs, 1339w, 1106b, 1029s, 841vs, 767w, 551m, cm^{-1}. ^{1}H NMR (CD_3CN): δ 2.8–4.1 (br, 24H, CH_3), 5.0 (br, 5H, Cp-H), 5.17 (wbr, 5H, Cp-H), 6.5–10.5 (br-m, 31H, Ar-H, Ph-H) ppm. Anal.: calcd. for $C_{67}H_{60}N_{12}S_8P_4F_{18}ZnRu_2$: C, 39.78; H, 2.96; N, 8.31; S, 12.66%. Found: C, 40.85; H, 2.21; N, 9.60; S, 11.97%.

Yield 6: 81 mg (37%). Λ_M (1.0×10^{-5} M): 300 $\Omega^{-1}cm^2\ mol^{-1}$. IR (KBr): ν 3439b, 1642vs, 1564s, 1413vs, 1347w, 1217w, 1098w, 1021s, 963s, 849vs, 767w, 555m, cm^{-1}. ^{1}H NMR (CD_3CN): δ 2.8–4.5 (br, 24H, CH_3), 4.99 (br, 5H, Cp-H), 5.18 (br, 5H, Cp-H), 6.5–10.5 (br-m, 31H, Ar-H, Ph-H) ppm. Anal.: calcd. for $C_{67}H_{60}N_{12}S_8P_4F_{18}ZnRu_2$: C, 39.78; H, 2.96; N, 8.31; S, 12.66%. Found: C, 39.60; H, 2.82; N, 8.51; S, 12.88%.

3. Results and discussion

[Zn{$(MeS)_8$TAP}] **1**, when reacted with equimolar amount of $[(bpy)_2RuCl_2]{\cdot}2H_2O$ resulted in peripheral (κ^2-S^2,S^3)[Ru^{II}] coordina-

tion forming dinuclear complex **2**. Whereas the reaction of **2** with equimolar amount of $[(phen)_2RuCl_2]\cdot 2H_2O$ or $[Cp(PPh_3)_2RuCl]$ yielded a mixture of two geometrical stereoisomers of trinuclear complexes **3**–**6** (Scheme 1). These cationic complexes were isolated as $[PF_6]^-$ salts and were separated by column chromatography over cellulose eluting with CH_2Cl_2/petroleum ether mixture. In case of trinuclear complexes two distinct bands were formed of which, the first band that moved faster was identified as the bent (κ^4-S^2,S^3,S^7,S^8)$[Ru^{II}]_2$ isomer, while the second band that moved slower was identified as the linear (κ^4-S^2,S^3,S^{12},S^{13})$[Ru^{II}]_2$ isomers on the basis of the spectral data [42]. Molar conductances of the complexes measured in dry acetone, indicated that complex **2** was a 2:1 electrolyte, **3**, **4** were 4:1 and **5**, **6** were 3:1 electrolytes [43]. Complexes are highly soluble in dichloromethane, acetone, and acetonitrile and are stable under ambient laboratory conditions.

3.1. ^1H NMR spectra

Due to poor solubility in $CDCl_3$ the ^1H NMR spectra of all complexes, except that of **1**, were recorded in CD_3CN. The complex **1** exhibited only one broad singlet at δ 3.04 ppm in its ^1H NMR spectra. As the molecule possesses only isolated —S—CH_3 groups, it was significantly broadened and downfield shifted under a strong anisotropic influence of TAP π-current and conformational fluxionality at thioether. The dinuclear complex **2**, and trinuclear complexes **3**–**6** exhibited two groups of signals, a broadened singlet between δ 2.8 and 4.5 ppm due to -S-CH_3 protons and a group of complex multiplets between δ 6.5 and 10.5 ppm due to aromatic bpy/phen/Ph protons. The observed spectra are indicative of the presence of peripherally bonded $Ru(bpy)_2$/$Ru(phen)_2$/$RuCp(PPh_3)$ units. The trinuclear complexes **5** and **6** possessing $RuCp(PPh_3)$ unit exhibited three groups of signals, i.e. two additional signals

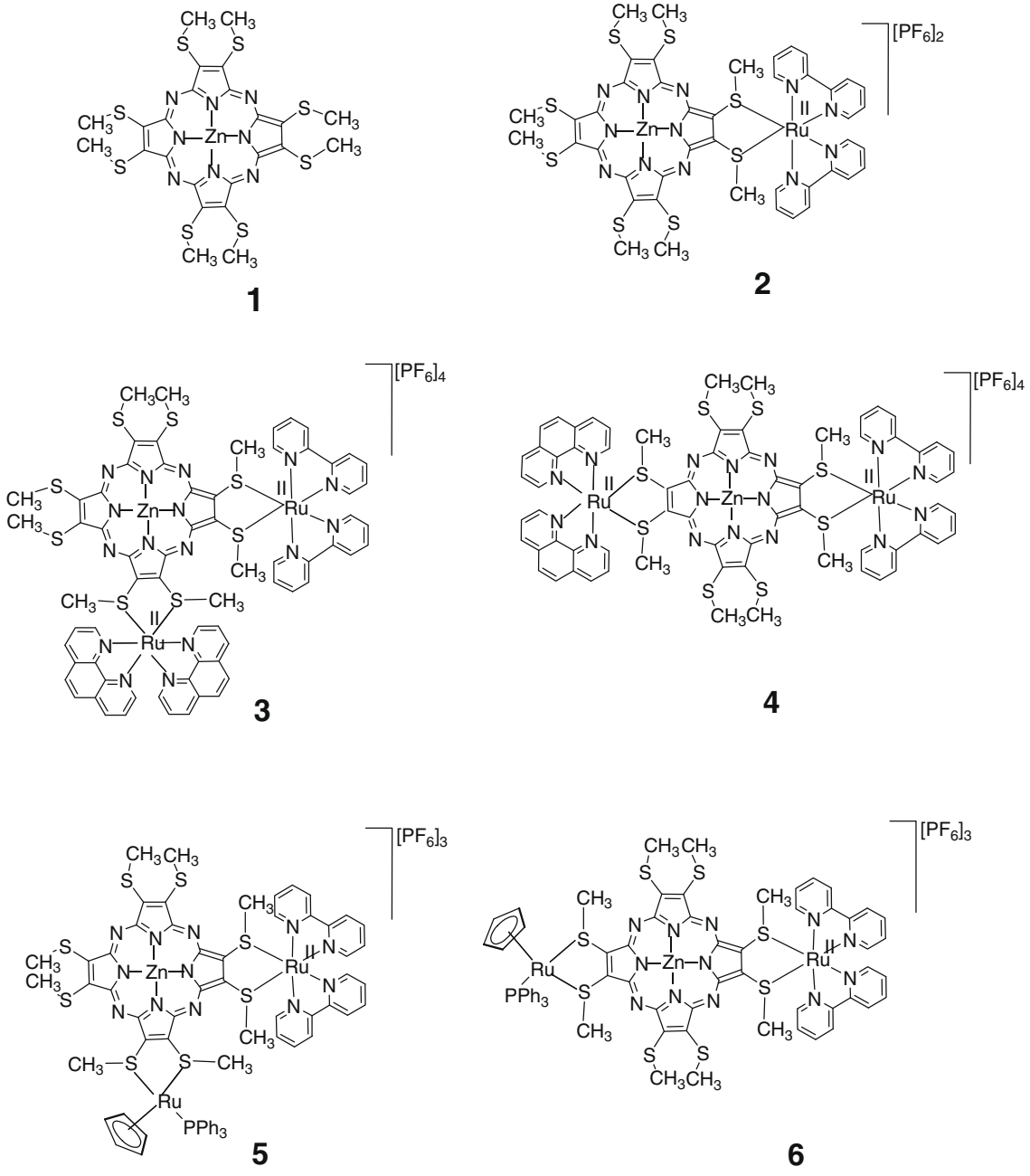

Scheme 1.

between δ 5.0 and 5.2 ppm, besides the —S—CH_3 and Ar-H signals, that are assigned to cyclopentadienyl protons [44]. Again the Cp-H signals are observed significantly downfield shifted as compared to other analogous thioether coordinated Ru(II)-Cp complexes [44,45] possibly due to additive anisotropic effects of the TAP and Cp ring currents.

The peripheral coordination of the $CpRu^{II}$ moiety was used as probe to differentiate between the two isomeric forms of the triads. The Cp-H signals in complexes **5** and **6**, observed between δ 5.0 and 5.2 ppm, were distinctly apart from other aromatic and alkyl group signals and hence were helpful in deducing structures of the isomers through ^{1}H NMR. The bent (κ^4-S^2,S^3,S^7,S^8)$[Ru^{II}]_2$ isomer **5**, exhibited a broad singlet while the linear (κ^4-S^2,S^3,S^{12},S^{13})$[Ru^{II}]_2$ isomer **6**, exhibited two signals with nearly equal intensity (Fig. 1). It is likely that these triad complexes existed in two conformational forms, i.e. *syn* and *anti* forms (Fig. 2). In either of the (κ^4-S,S′,S″,S‴)$[Ru^{II}]_2$ thioether coordination the two peripheral Ru(II) units reside slightly off the TAP ring plane, being either on the same side (*syn*-form) or on the opposite sides (*anti*-form). In case of the bent (κ^4-S^2,S^3,S^7,S^8)$[Ru^{II}]_2$ complex, because of strong steric interaction between the two bulky peripheral Ru(II) units, the *anti* stereoisomer is likely to predominate over the *syn* stereoisomer thus giving only one Cp-H signal.

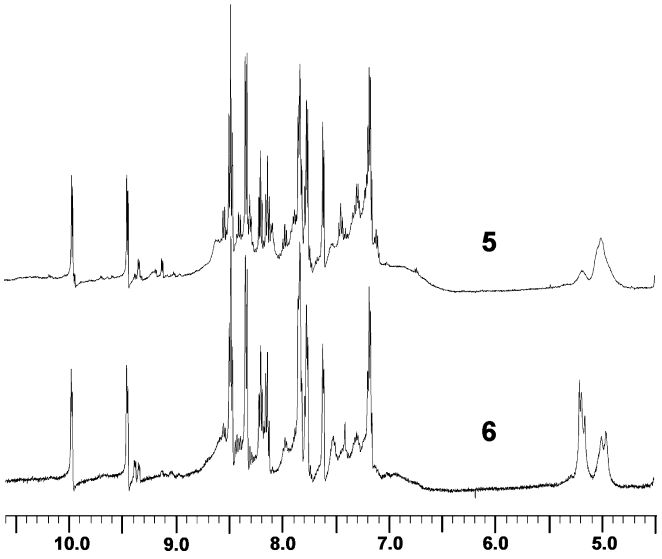

Fig. 1. ^{1}H NMR spectra of complexes **5** and **6** in CH_3CN-d_3.

On the other hand, in the linear (κ^4-S^2,S^3,S^{12},S^{13})$[Ru^{II}]_2$ complex the two bulky peripheral Ru(II) units are spatially at longer distance from each other and hence exert weaker mutual steric interaction leading to formation of *syn* and *anti* stereomers in nearly comparable amounts. As seen from Fig. 1, the complex **5** exhibited a strong singlet Cp-H signal at δ 5.0 ppm, with another very weak singlet at δ 5.2 ppm, having peak area < 10% of the former. Hence the triad complex **5** has been assigned bent structure and the complex **6** that exhibited two Cp-H signals at δ 5.2 and δ 5.0 ppm with integral peak area ratio 55:45 in this region has been assigned a linear structure. The assigned structures are in agreement with their shape dependent elution behaviour on the column (with former being near spherical moved faster).

The aromatic proton signals in the isomeric pair **5** and **6** as well as in **3** and **4** between δ 6.5 and 10.5 ppm were difficult to assign to individual protons, in absence of correlation studies, though they were qualitatively distinct from each other. The assignments of the linear and bent structures to complexes **3** and **4** are made by comparing their other properties, *viz.*, column movement behaviour, voltammetry and fluorescence lifetime data vis-à-vis that of complexes **5** and **6**.

3.2. Mass spectra

The mass spectra of the complexes were quite helpful in deducing molecular structures. The fast atomic bombardment (FAB) led to excessive fragmentation in dyad and triad complexes, therefore only the complex **1**, was studied by FAB-MS while others were studied in the MALDI-TOF mass spectra, in a matrix consisting of 2,5-dihydroxy benzoic acid (DHB) dissolved in $CHCl_3$. The molecule ion peak in complex **1**, was observed at *m*/*z* 745, while, the di- and

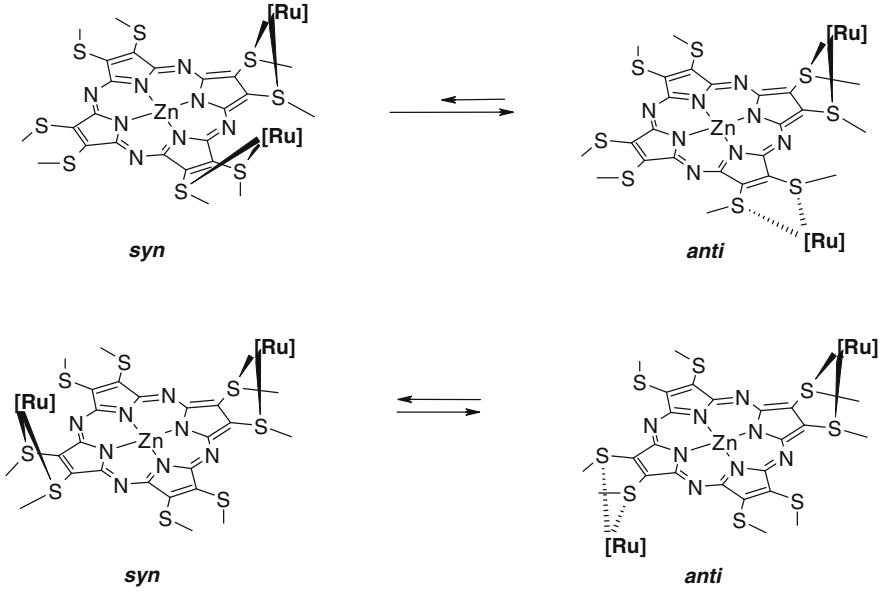

Fig. 2. Conformational forms of bent (κ^4-S^2,S^3,S^7,S^8)$[Ru^{II}]_2$ and linear (κ^4-S^2,S^3,S^{12},S^{13})$[Ru^{II}]_2$ triads.

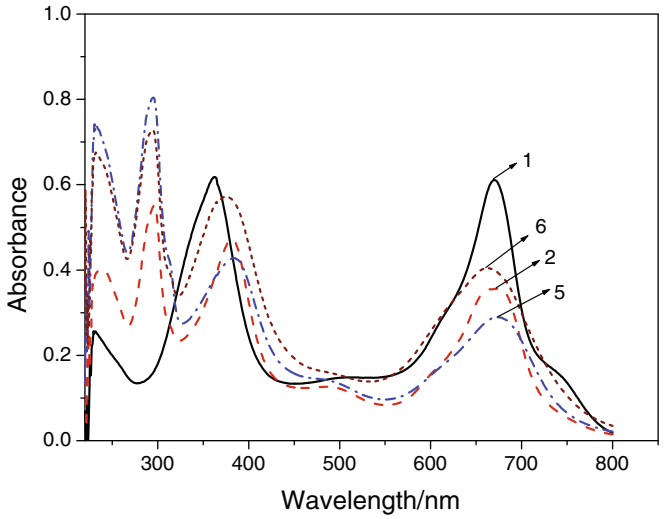

Fig. 3. Electronic absorption spectra of 1.0×10^{-5} M solution of the complexes **1, 2, 5** and **6** in CH_2Cl_2.

trinuclear complexes exhibited weak ion peaks between 695–703, 1057–1063, 1096–1102, 1008–1014, and 1093–1100 due to formation of $[\mathbf{2}+2CHCl_3\text{-}2PF_6]^{2+}$, $[\mathbf{3}+3CHCl_3\text{-}3PF_6]^{2+}$, $[\mathbf{4}]^{2+}$, $[\mathbf{5}]^{2+}$ and $[\mathbf{6}+3DHB\text{-}2PF_6]^{2+}$ molecule ions, respectively. Since ruthenium consists of several natural isotopes with masses 96–104 it gives a characteristic signature to the fragments where it is present.

Invariably the base ion peak was observed between 561–568, 611–616 and 697–704 in all complexes that correspond to $[Ru^{II}(bpy)_2+DHB]^+$, $[Ru^{II}(phen)_2+DHB]^+$ and $[(PPh_3)CpRu^{II}+DHB+CHCl_3]^+$ fragments, respectively. Some additional fragment peaks were observed, e.g. in complex **3**, between 783 and 789 due to formation of $[Ru(phen)_3+PF_6]^+$ and in complex **4**, between 970 and 977 due to formation of $[\mathbf{4}\text{-}Ru^{II}(bpy)_2\text{-}PF_6+2DHB]^{2+}$ fragments.

3.3. Electronic spectra

The electronic spectra of complexes **1–6** were recorded in CH_2Cl_2. They all exhibited two major bands, a longer wavelength Q-band and a shorter wavelength Soret band, characteristic of tetraazaporphyrins (TAP's). However, unlike that in [Zn(porph)] [46,47] the Soret and Q-bands in complex **1** were of nearly equal intensity. Also there appeared a relatively weak absorption band at *ca.* 475 nm due to N_{meso}–π^* transitions. Complexes **2–6** also exhibited two additional bands, one relatively weak absorption band between λ_{max} 480 and 490 nm due to MLCT [$d\pi(Ru) \rightarrow \pi^*$(bpy)/(phen)] transition and the second strong absorption band between λ_{max} 267 and 297 nm due to intraligand π–π^*(bpy)/(phen) transitions vis-à-vis complex **1**, besides the strong Soret and Q-bands, (Fig. 3). Peripheral binding of the first $(bpy)_2Ru^{II}$ unit led to moderate hypsochromic shift in the Q-band maxima in the dinuclear complex **2**, but upon binding of the second Ru(II) unit it was markedly bathochromic shifted in the trinuclear complexes **3–6**. The shifts in the band maxima apparently arose from the combined effects of (1) lowered symmetry due to peripheral metal binding and (2) distortion of the TAP ring plane as a consequence of steric effects. A semiquantitative calculation of relative HOMO, LUMO energies in metallo-tetraazaporphyrins using theoretical methods suggest relative change in the orbital energies [48,49]. The $(\kappa^2\text{-}S^2,S^3)[Ru^{II}]$ coordination leads to change in molecular symmetry from D_{4h} to C_{2v}, while in the trinuclear complexes different conformational forms of the bent $(\kappa^4\text{-}S^2,S^3,S^7,S^8)[Ru^{II}]_2$ and linear $(\kappa^4\text{-}S^2,S^3,S^{12},S^{13})[Ru^{II}]_2$ isomers bear C_{2v} or C_2 symmetry. The lowered symmetry in these complexes resulted in lifting of the degeneracy of the LUMO e_g levels in the TAP core. The HOMO and HOMO-1 now no longer have different symmetry and due to configuration interaction get energetically separated from each other. Splitting of the LUMO and HOMO levels results into four transitions having lowered configuration interactions and thereby led to a shift in Q and Soret band positions. In the linear $(\kappa^4\text{-}S^2,S^3,S^{12},S^{13})[Ru^{II}]_2$ trinuclear complex **6** Q-band showed a more noticeable hypsochromic shift, observed at λ_{max} 662.0 nm as compared to the dinuclear complex **2** that was absorbed at λ_{max} 667.0 nm (Fig. 3). The $Cp(PPh_3)Ru^{II}$ moiety being relatively bulkier is likely to exert higher steric effect than $(phen)_2Ru^{II}$ and $(bpy)_2Ru^{II}$ moieties. This leads to greater distortion in the TAP planarity causing hypsochromic shift of Q-band in complex **6**.

3.4. Cyclic voltammetry

Cyclic voltammogram of complex **1**, was recorded in dry benzene/acetonitrile (1:1 v/v) mixture due to solubility reason, while that of complexes **2–6** were recorded in acetonitrile solutions and observed data are summarized in Table 1. The complex **1**, exhibited two reversible one electron reduction waves at $E_{1/2}$ −0.34 and −0.60 V and a third irreversible one at $E_{p,c}$ −1.35 V *vs.* Ag/AgCl due to ring centered reductions of the [Zn{$(MeS)_8$TAP}] core.

However, unlike in the mononuclear [Zn{$(MeS)_8$TAP}] **1**, the dinuclear complex **2**, exhibited only one reversible reduction wave at $E_{1/2}$ −0.58 V *vs.* Ag/AgCl, and no other wave was observed up to −1.0 V (Fig. 4). It appears that peripheral binding of Ru(II) units resulted into shift in the two reduction waves closer to each other, such that they coalesced into apparently one wave. Relative peak currents are indicative of this effect (Fig. 4). The peripheral coordination of the second Ru(II) moiety in the trinuclear complexes led to a shift in the reduction wave to more positive potential, vis-à-vis that in corresponding dinuclear complex. The trend is in conformity with the expected destabilization of the {$(MeS)_8$TAP} LUMO levels. Partly it is also due to enhanced overall positive charge on the complex. The reduction of the coordinated bipyridyl/phenanthroline units were observed as a quasi reversible wave between −1.40 and −1.60 V *vs.* Ag/AgCl in all complexes.

Table 1
Electronic spectral and cyclic voltammerty data of complexes **1–6**.

Compounds	Absorption spectra, λ_{max}/nm ($\log \varepsilon_{max}$)	$E_{1/2}$, V (*vs* Ag/AgCl)	
		Redn.	Oxidn.
1	670.5(4.78),475(4.14), 363.0(4.79)	−0.34, −0.60, −1.35	1.57(irr.)
2	667.0(4.55), 482.5(4.10), 381.0(4.67), 296.5(4.74), 239.0(4.60)	−0.58	0.62, 1.18
3	673.0(4.55), 483.0(4.27), 390.0(4.69), 291.5(4.87), 268.5(4.93), 231.0(4.92)	−0.56	0.61, 0.88, 1.16
4	675.0(4.58), 487.0(4.33), 389.5(4.72), 287.5(4.91), 268.5(4.98), 231.5(4.95)	−0.57	0.62, 1.17
5	672.5(4.46), 488.0(4.15), 383.5(4.63), 295.0(4.90), 230.5(4.87)	−0.56	0.61, 0.90, 1.15, 1.41(irr)
6	662.0(4.60), 484.0(4.20), 374.0(4.75), 294.5(4.86), 231.5(4.82)	−0.57	0.62, 1.16 1.43(irr)

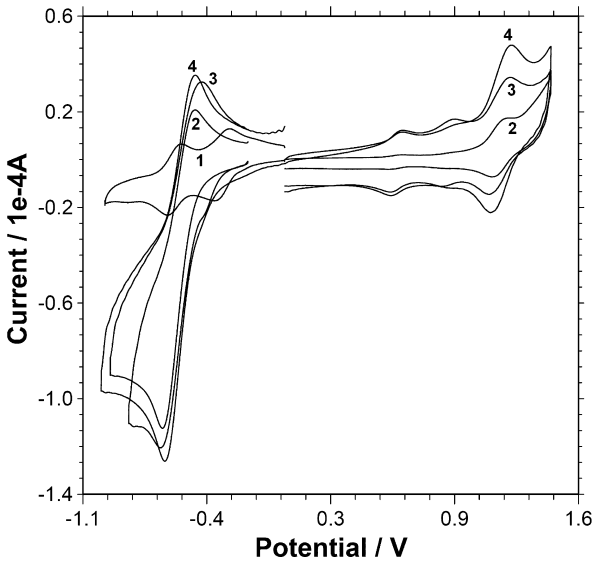

Fig. 4. Cyclic voltammograms of [Zn{(MeS)$_8$TAP}], **1** in benzene/acetonitrile (1:1, v/v) mixture and **2**–**4** in acetonitrile at glassy carbon working electrode in presence of 0.1 M TEAP supporting electrolyte (scan rate 200 mV/s).

In the oxidative voltammetry scans trinuclear complexes exhibited multiple reversible oxidation waves, unlike the one wave observed in complex **1**. The complex **1**, exhibited an irreversible oxidation at $E_{p,a}$ 1.57 V, attributable to {(MeS)$_8$TAP} ring oxidation. But upon binding of one (bpy)$_2$Ru^{II} metal moiety, in dinuclear complex, two reversible oxidations were observed in **2** at $E_{1/2}$ 0.62 and 1.18 V *vs.* Ag/AgCl. A comparison of the oxidative voltammograms of complexes **2**, **3** and **4** is shown in Fig. 4. Closer look reveals that the first oxidation wave has very poor electrode activity in **2**. However, upon binding of the second Ru(II) unit to obtain linear (κ^4-S^2,S^3,S^{12},S^{13})[Ru^{II}]$_2$ triad, **4** the electrode activity of the first wave improved significantly, while in the bent (κ^4-S^2,S^3,S^7,S^8)[Ru^{II}]$_2$ triad, **3** there appeared an additional reversible oxidation wave at $E_{1/2}$ 0.88 V in between the two other oxidation waves at $E_{1/2}$ 0.61 and 1.16 V. Similarly the other bent (κ^4-S^2,S^3,S^7,S^8)[Ru^{II}]$_2$ triad **5** also exhibited three oxidation waves. The lowest potential oxidation wave in the di- and trinuclear complexes is likely to arise from Ru(II)/Ru(III) process while the reversible wave between $E_{1/2}$ 1.15 and 1.18 V is likely to arise from {(MeS)$_8$TAP}/{(MeS)$_8$TAP}$^+$ process, which is inconformity with the oxidation of **1**. The second oxidation of the {(MeS)$_8$TAP} ring in these complexes was also observed, but as an irreversible wave between E_p 1.41 and 1.43 V. Compared to saturated bis(thioether) coordinated (bpy)$_2$Ru^{II} complexes [50], the Ru(II) oxidation in these complexes is much easier and is only moderately above that of Cl^- complexes [51], indicating greatly diminished π-acid effect of the β-thioethers at the {(MeS)$_8$TAP} ring. However, the poor π-acid effect is not uncommon with alkenic thioether complexes [44,52].

The presence of one and two Ru(II) centered oxidations in linear and bent complexes is rather intriguing. We have tentatively attributed the fact to independent redox behaviour of the two peripheral Ru(II) units in linear complexes, but formation of delocalized and successive oxidation of Ru(2.5+)–Ru(2.5+) state in the bent complexes. Low peak currents might be due to low value of heterogeneous electron transfer coefficient to the electrode. Thus in the linear complexes the two Ru(II) centers were oxidized at the same potential, while in the latter (bent complexes) the first oxidation led to formation of Ru(2.5+)–Ru(2.5+) delocalized state which was subsequently oxidized at a more positive potential, $E_{1/2}$ 0.88 V, to Ru(III)–Ru(III) state. The first {(MeS)$_8$TAP} centered oxidation in all polynuclear complexes **2**–**6** were easier to effect than that in the precursor complex **1**, despite of enhanced positive charge on it. The effect seems to arise (i) due to destabilization of the {(MeS)$_8$TAP} HOMO and HOMO-1 levels or (ii) due to improved solvation of the cationic complexes. It is logically expected that the solvation effect has dominated.

3.5. Luminescence study

Photophysical properties of the precursor complex **1** and its dyad and triad derivatives, **2**–**6** were investigated in dichloromethane, a non-coordinating solvent. Dilute 1.0×10^{-5} M solutions were used to avoid self-quenching. Since these consisted of two different chromophore units, *viz.*, [Zn{(MeS)$_8$TAP}] and (bpy)$_2$Ru^{II}/(phen)$_2$Ru^{II} both of which are proven luminophores, energy transfers from one to another unit within the molecule and vice versa were anticipated to dominate visible light emissions. In fact these

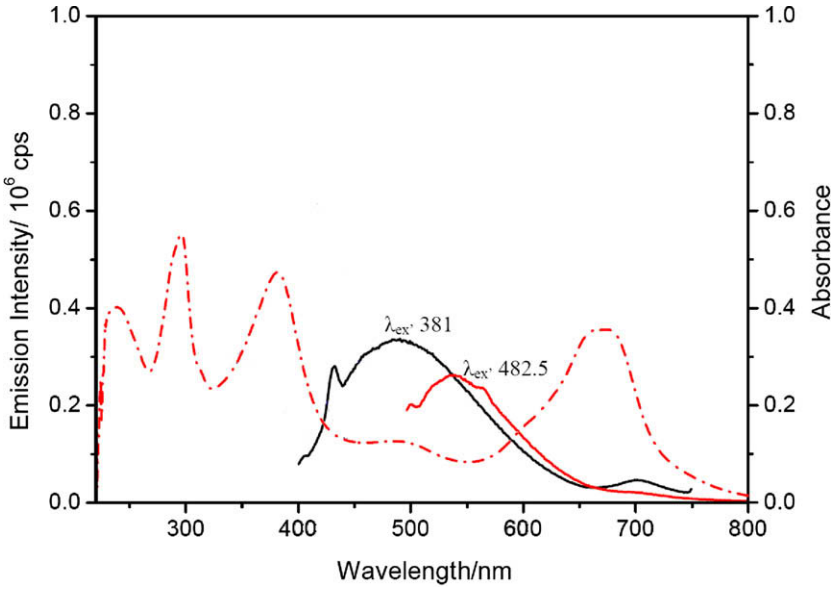

Fig. 5. Fluorescence emission spectra (-) at different excitation wavelengths and electronic absorption spectra (-·-) of complex **2** in CH_2Cl_2.

Table 2
Fluorescence spectral data of complexes **1**–**6**.

Compounds	Emission spectra		Excitation spectra	
	λ_{exc}/nm	$\lambda_{max,em}$/nm	λ_{em}/nm	$\lambda_{max,exc}$/nm
1	670.5	N.E.	537	368,412sh
	475.0	537	407	359
	363.0	407	430	381
			459	402
2	667.0	N.E	536	323w, 431sh, 475sh
	482.5	536	563	350, 422w, 478sh
	381.0	432	432	311, 338sh, 380
		459	459	317, 361sh, 403
		489	489	321w, 363sh, 423
			519	321w, 429sh, 472
			701	381w
3	673.0	N.E	538	323, 366, 420, 460sh
	483.0	538	582	310, 362, 435sh
	390.0	443	443	350sh, 388
		501	501	360sh, 412
		533	533	325, 365w, 416sh
			572	432, 520sh
4	675.0	N.E	539	322, 424, 461sh
	487.0	539	568	355, 425w, 466sh
	389.5	442	442	352sh, 386
		466	466	353w, 408sh
		498	498	323w, 361, 429sh
			529	324, 363, 423, 454sh
			566	344, 418w, 485sh
5	672.5	N.E	538	324, 425, 460sh
	488.0	538	572	321, 427, 521sh
	383.5	572	435	326sh, 358, 381
		435	481	325w, 365, 418
		481	573	321w, 428, 520sh
6	662.0	N.E	540	319, 422, 463sh
	484.0	540	567	308, 351, 420, 485sh
	374.0	567	422	335w, 370w
		422	478	322, 369, 416
		478	673	374w
		673		

N.E.: non-emitting, w: weak, sh: shoulder.

Table 3
Lifetime characteristics of the emitting states of complexes **1**–**6**.

Compounds	Emission spectra		Life time in ns (% contribution)
	λ_{exc}/nm	$\lambda_{max,em}$/nm	
1	475.0	537	3.58 (98.34), 0.0012 (1.67)
	363.0	407	9.49 (11.64), 1.39 (88.34)
		430	7.71 (19.87), 1.39 (80.13)
2	482.5	536	8.55 (32.88), 2.91 (67.12)
		563	8.62 (37.00), 2.83 (63.00)
		432	9.83 (23.20), 2.20 (76.80)
	381.0	489	9.73 (28.14), 2.34 (71.86)
		701	7.07 (15.52), 1.37 (84.48)
3	483.0	538	10.69 (15.82), 3.15 (84.18)
		582	10.11 (29.71), 2.91 (70.29)
	390.0	501	13.27 (39.20), 3.27 (60.80)
		572	13.65 (23.82), 2.77 (76.18)
4	487.0	539	9.68 (26.51), 2.99 (73.49)
		568	10.96 (24.50), 2.69 (75.50)
	389.5	498	11.17 (25.80), 2.68 (74.20)
		566	10.39 (30.00), 2.56 (69.99)
5	488.0	538	10.46 (13.91), 3.35 (86.09)
		572	9.09 (27.37), 3.09 (72.68)
	383.5	435	7.98 (41.31), 1.97 (58.70)
		481	7.92 (44.50), 1.97 (55.50)
6	484.0	540	10.19 (9.50), 3.25 (90.50)
		567	9.23 (15.74), 3.20 (84.26)
	374.0	478	7.57 (41.84), 1.72 (58.16)
		673	7.44 (38.96), 1.92 (61.04)

supramolecular systems exhibited luminescence features that were hybrid of the two constituent units and indicated presence of strong inter component electronic communication.

Upon Q-band excitation of these complexes no detectable emission were observed at longer wavelength up to 800 nm suggesting dominance of radiationless deactivation of the S_1 state. However, the Soret and $(bpy)_2Ru^{II}$/$(phen)_2Ru^{II}$ centered MLCT excitations led to strong visible region emissions. The Soret excitation, particularly in complexes **2** and **6** also led to a very weak S_1 emission.

The strong S_2 emission in the visible region and the non-radiative S_1 state were the most important features of these complexes. Unlike porphyrins that primarily emit through S_1 state [53,54] (although there are a few reports on porphyrin S_2 emission [54–58]) S_2 emission in metallo-tetraazaporphyrins is not uncommon [31,32,59,60]. Also the S_2 state in these complexes exhibited relatively longer lifetime (τ 2.00–3.60 ns) than the S_2 state in metallo-porphyrin (τ 0.38 ± 0.01 ps) [61]. The excitation maxima of the 407 nm emission in [Zn{$(MeS)_8$TAP}] coincided with the Soret absorption maxima, indicating its origin to this excitation. Upon binding of a $(bpy)_2Ru^{II}$ moiety to [Zn{$(MeS)_8$TAP}], in complex **2** emission maxima was shifted to longer wavelengths 432 nm (Figs. 5 and 6). When the selected emission wavelength in complex **2** was changed to 459 and 489 nm the excitation maxima also got moderately shifted to longer wavelength side indicating enhanced excitatory contribution from the peripheral $(bpy)_2Ru^{II}$ moiety's

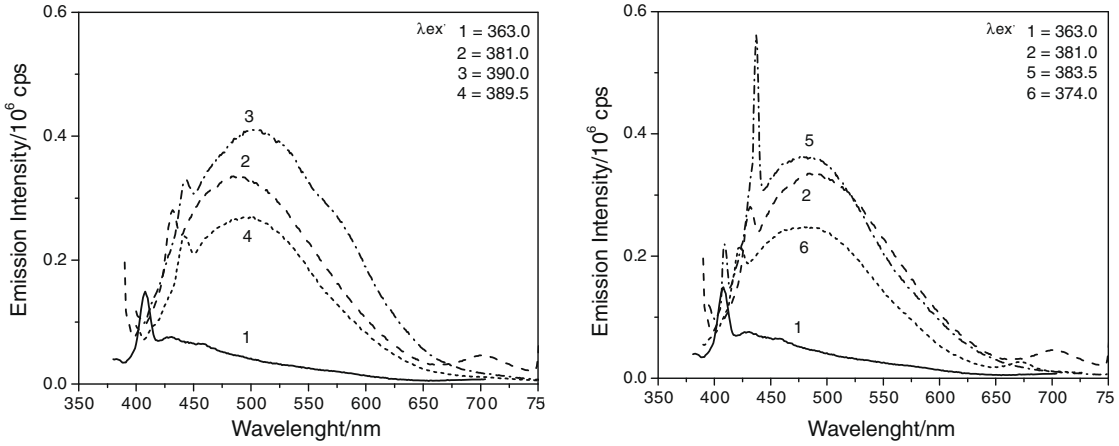

Fig. 6. Fluorescence emission spectra of 1.0×10^{-5} M solution (Soret excitation) of complexes **1**–**6** in CH_2Cl_2.

LMCT absorption. In addition, these complexes exhibited a new emission maxima between $\lambda_{em,max}$ 535–545 nm, e.g. $\lambda_{em,max}$ 536 for λ_{ex} 482.5 in complex **2** corresponding to MLCT excited state (Table 2) (Fig. 5).

Life time decay analysis of 537 nm emission in complex **1** showed a predominant (98.3%) contribution from τ 3.58 ns with only 1.7% contribution from τ 1.2 ps (Table 3). However, upon binding of $(bpy)_2Ru^{II}$ moiety in the dinuclear complex **2** for the corresponding emission maxima at λ_{em} 536 the contribution of the

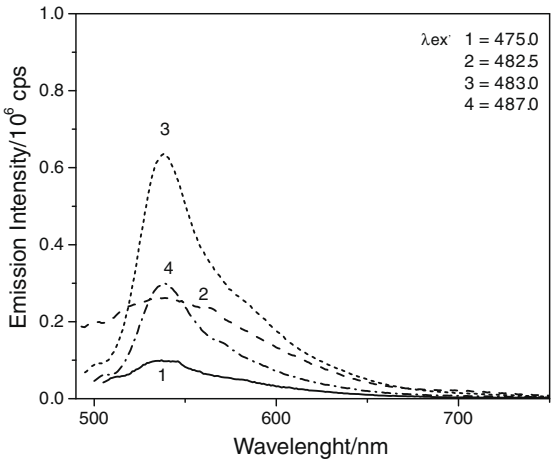

Fig. 7. Fluorescence emission spectra of 1.0×10^{-5} M solution (MLCT excitation) of complexes **1**–**4** in CH_2Cl_2.

$[Zn\{(MeS)_8TAP\}]^*$ centered dominant emitting state decreased to 67.1% with moderate shortening of the lifetime to 2.91 ns. Also there emerged a new emitting state with significantly longer lifetime τ 8.55 ns (32.9%) in **2**. The second emitting state seems to arise in the peripheral $(bpy)_2Ru^{II}$ emission. The emission data of the precursor $[Zn\{(MeS)_8TAP\}]$ and $(bpy)_2Ru^{II}$ units indicated that the excited states in the two linked moieties were of comparable energies and had a moderate (<8.5 kJ mol^{-1}) energy barrier.

The emission spectra of the equimolar solutions of complexes **1**–**6** for Soret absorption and complexes **1**–**4** for MLCT absorption are shown in Figs. 6 and 7. From the Fig. 6 it could be easily seen that emission efficiency in complex **1** is significantly lower as compared to other di and trinuclear complexes. Complex **2** exhibited nearly three times higher emission intensity than complex **1** at the same molar concentration. Upon binding of the second Ru(II) unit in the linear $(\kappa^4\text{-}S^2,S^3,S^{12},S^{13})[Ru^{II}]_2$ trinuclear complexes emissivity decreased moderately, but it is further increased in the bent $(\kappa^4\text{-}S^2,S^3,S^7,S^8)[Ru^{II}]_2$ trinuclear complexes. In fact the observed S_2 emission intensity in the linear $(\kappa^4\text{-}S^2,S^3,S^{12},S^{13})[Ru^{II}]_2$ isomers were nearly half of that in corresponding bent $(\kappa^4\text{-}S^2,S^3,S^7,S^8)[Ru^{II}]_2$ isomers. Difference in the emission intensities of di- and trinuclear complexes arose from difference in the electronic communication between the components with low energy barrier and also due to differing efficiencies of radiationless deactivation pathways. In the linear $(\kappa^4\text{-}S^2,S^3,S^{12},S^{13})[Ru^{II}]_2$ isomers the two Ru(II) moieties lie opposite to each other cancelling their mutual dipoles, unlike that in bent $(\kappa^4\text{-}S^2,S^3,S^7,S^8)[Ru^{II}]_2$ isomers. Furthermore, due to elongated structure the linear $(\kappa^4\text{-}S^2,S^3,S^{12},S^{13})[Ru^{II}]_2$ molecules also had greater chance of competing collisional loss of the absorbed energy than the bent $(\kappa^4\text{-}S^2,S^3,S^7,S^8)[Ru^{II}]_2$ molecules with nearly spherical shape. Thus

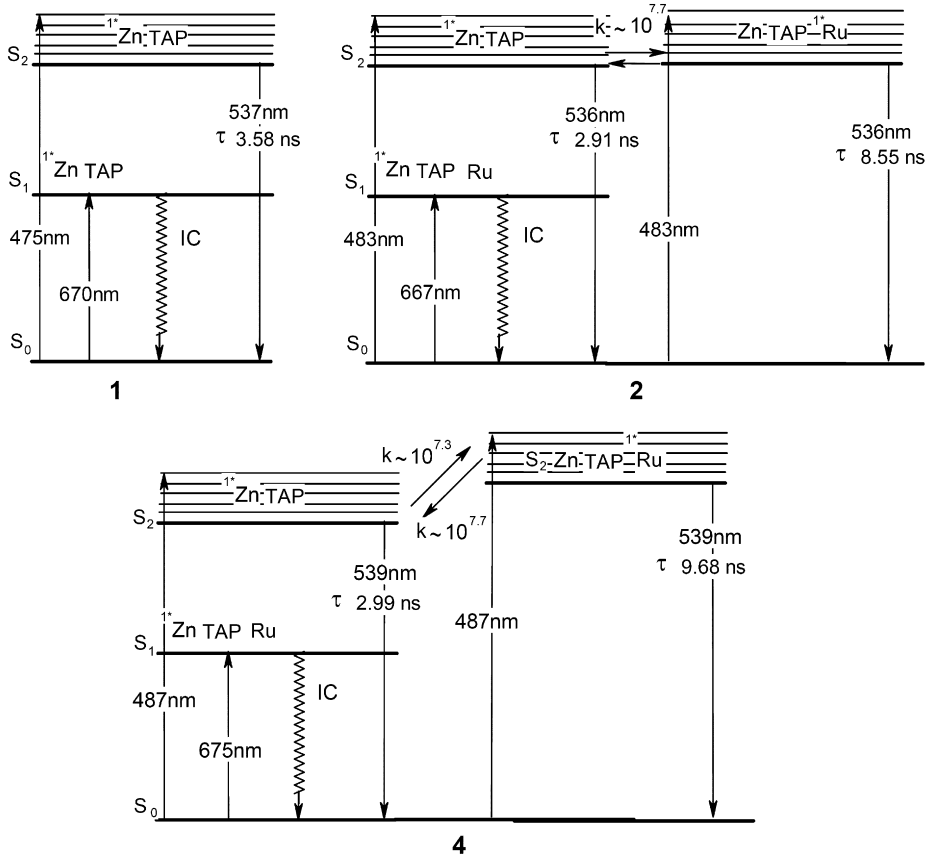

Fig. 8. Schematic energy level diagram showing dynamics of excited state energy transfer in $[Zn\{(MeS)_8TAP\}]$, **1**, dinuclear $[Zn\{(MeS)_8TAP\}\text{-}Ru(bpy)_2]^{2+}$, **2** and linear trinuclear $[Zn\{(MeS)_8TAP\}\{Ru(bpy)_2\}\{Ru(phen)_2\}]^{4+}$, **4** complexes.

binding of second Ru(II) unit to TAP core in bent (κ^4-S^2,S^3,S^7,S^8)$[Ru^{II}]_2$ configuration led to stronger TAP S_2 fluorescence.

The S_2 emission in the trinuclear complexes also showed two exponential decays, similar to that in the dinuclear complex **2**. However, the Zn^{II}-{$(MeS)_8$TAP}* component emission lifetime was moderately shortened and the $(bpy)_2Ru^{II}$/$(phen)_2Ru^{II*}$ component emission lifetime was moderately lengthened upon formation of the trinuclear complexes. Also the bent (κ^4-S^2,S^3,S^7,S^8)$[Ru^{II}]_2$ complexes showed invariably longer lifetimes and stronger fluorescence intensity than corresponding linear (κ^4-S^2,S^3,S^{12},S^{13})$[Ru^{II}]_2$ counterparts. The lifetime data also shows that emission contribution from $(bpy)_2Ru^{II}$/$(phen)_2Ru^{II*}$ moieties in the trinuclear complexes, **3**–**6** are significantly lower than that in the dinuclear complex **2** (Table 3). It could be explained through a semiquantitative energy level diagram as shown in Fig. 8. It is likely that binding of the first Ru(II) unit created two emitting states Zn^{II}-{$(MeS)_8$TAP}*-$(bpy)_2Ru^{II}$ and Zn^{II}-{$(MeS)_8$TAP}-$(bpy)_2Ru^{II*}$ with comparable energies, but upon binding of the second Ru(II) unit the Zn^{II}-{$(MeS)_8$TAP}*-$(bpy)_2$Ru state got stabilized so that it became the principal emitting state [62]. The Zn^{II}-{$(MeS)_8$TAP}* emission lifetimes in the bent isomers were invariably longer than that in the linear isomers. This is in agreement with the assigned shapes of the molecules and thereby effectiveness of the collisional deactivation.

Acknowledgments

Authors are thankful to the University Grants Commission, New Delhi (India) for financial support through Grant No. F. No.10-2(5)2003(I)-EU.II. (R.K.) and to FST, the University of the South Pacific through Grant Code 6C141-1321 (R.P.). We are also thankful to Head, RSIC CDRI, Lucknow, India for recording mass spectra of all these compounds.

References

[1] W. Jones, C.N.R. Rao (Eds.), Supramolecular Organization and Materials Design, Cambridge University Press, 2002.
[2] D. Porath, Y. Levi, M. Tarabiah, O. Millo, Phys. Rev. B 56 (1997) 9829.
[3] L.A. Bamm, J.J. Arnold, M.T. Cygan, T.D. Dunbar, T.P. Burgin, L. Jones II, D.L. Allara, J.M. Tour, P.S. Weiss, Science 271 (1996) 1705.
[4] A. Bezryadin, C. Dekker, J. Vac. Sci. Tech. B 15 (1997) 793.
[5] H. Park, A.K.L. Lim, A.P. Alivisatos, P.L. McEuen, Appl. Phys. Lett. 75 (1999) 301.
[6] A.F. Morpurgo, C.M. Marcus, D.B. Robinson, Appl. Phys. Lett. 74 (1999) 2084.
[7] P. Nuguyen, P. Ǵomez-Elipe, I. Manners, Chem. Rev. 99 (1999) 1515.
[8] A.S. Abd-El-Aziz, E.K. Todd, Coord. Chem. Rev. 246 (2003) 3.
[9] I. Manners, Synthetic Metal-Containing Polymers, Wiley, Weinheim, 2004. p. 153 (Chapter 5).
[10] A.S. Abd-El-Aziz, Macromol. Rapid Commun. 23 (2002) 995.
[11] R.P. Kingsborough, T.M. Swager, Prog. Inorg. Chem. 48 (1999) 123.
[12] C. Janiak, Dalton Trans. (2003) 2781.
[13] I. Goldberg, Chem. Eur. J. 6 (2000) 3863.
[14] Y. Diskin-Posner, S. Dahal, I. Goldberg, Angew. Chem. Int. Ed. 39 (2000) 1288.
[15] R.K. Kumar, Y. Diskin-Posner, I. Goldberg, Inorg. Chem. 37 (1998) 541.
[16] H. Imahori, Org. Biomol. Chem. 2 (2004) 1425.
[17] S. Lee, A.J.P. White, D.J. Williams, A.G.M. Barrett, B.M. Hoffman, J. Org. Chem. 66 (2001) 461.
[18] M.E. Anderson, A.G.M. Barrett, B.M. Hoffman, J. Inorg. Biochem. 80 (2000) 257.
[19] F.S. Fouad, C.F. Crasto, Y. Lin, G.B. Jones, Tetrahedron Lett. 45 (2004) 7753.
[20] J. Golab, G. Wilczynski, R. Zagozdzon, T. Stoklosa, A. Dabrowska, J. Rybczynska, M. Wasik, E. Machaj, T. Oldak, K. Kozar, R. Kaminski, A. Giermasz, A. Czajka, W. Lasek, W. Feleszko, M.J. Jakobisiak Br, Cancer 82 (2000) 1485.
[21] S.V. Kudrevich, J.E. van Lier, Coord. Chem. Rev. 156 (1996) 163.
[22] R.M. Christie, B.G. Freer, Dyes Pigm. 33 (1997) 107.
[23] V.F. Slagt, P.C.J. Kamer, P.W.N.M. Van Leeuwen, J.N.H. Reek, J. Am. Chem. Soc. 126 (2004) 1526.
[24] K. Araki, H. Winnischofer, H.E.B. Viana, M.M. Toyama, F.M. Engelmann, I. Mayer, A.L.B. Formiga, H.E. Toma, J. Electroanal. Chem. 562 (2004) 145.
[25] M.L. Merlau, W.J. Grande, S.T. Nguyen, J.T. Hupp, J. Mol. Catal. A: Chem. 156 (2000) 79.
[26] M. Kawa, Top. Curr. Chem. 228 (2003) 193.
[27] P.A. Liddell, G. Kodis, J. Andreasson, L. De la Garza, S. Bandyopadhyay, R.H. Mitchell, T.A. Moore, A.L. Moore, D. Gust, J. Am. Chem. Soc. 126 (2004) 4803.
[28] S.A. Vail, J.P.C. Tome, P.J. Krawczuk, A. Dourandin, V. Shafirovich, J.A. S Cavaleiro, D.I. Schuster, J. Phys. Org. Chem. 17 (2004) 814.
[29] O. Hagemann, M. Jorgensen, F.C. Krebs, J. Org. Chem. Article (2006).
[30] M. Oda, H. Matsumura, Jpn. Kokai Tokkyo Koho (2004).
[31] R. Prasad, A. Kumar, Inorg. Chim. Acta 358 (2005) 3201.
[32] R. Prasad, A. Kumar, J. Porphyrins Phthalocyanines 9 (2005) 509.
[33] R. Prasad, E. Murguly, N.R. Branda, Chem. Commun. (2003) 488.
[34] R. Prasad, A. Kumar, E. Murguly, N.R. Branda, Inorg. Chem. Commun. 4 (2001) 19.
[35] R. Prasad, V.K. Gupta, A. Kumar, Anal. Chim. Acta 508 (2004) 61.
[36] R. Prasad, A. Kumar, J. Electroanal. Chem. 576 (2005) 295.
[37] R. Prasad, A. Kumar, V.K. Gupta, Talanta 63 (2004) 1027.
[38] C.J. Schramm, B.M. Hoffman, Inorg. Chem. 19 (1980) 383.
[39] B.P. Sullivan, D.J. Salmon, T.J. Meyer, Inorg. Chem. 17 (1978) 3334.
[40] M.I. Bruce, N.J. Windsor, Aust. J. Chem. 30 (1977) 1601.
[41] J. Nocedal, S.J. Wright, Numerical Optimization, Springer, New York, 1999.
[42] R. Kumar, A. Kumar, R. Prasad, Transition Met. Chem. 32 (2007) 1091.
[43] W.J. Geary, Coord. Chem. Rev. 7 (1971) 81.
[44] R. Prasad, J. Organomet. Chem. 486 (1995) 31.
[45] R. Prasad, Polyhedron 14 (1995) 2151.
[46] M.J. Stillman, T. Nyokong, in: C.C. Leznoff, A.B.P. Lever (Eds.), Phthalocyanines: Properties and Applications, vol. 1, VCH, New York, 1989 (Chaper 3).
[47] M. Gouterman, in: D. Dolphin (Ed.), The Porphyrins, vol. III, Academic Press, New York, 1978, pp. 1–165.
[48] J. Mack, M.J. Stillman, Coord. Chem. Rev. 219 (2001) 993.
[49] E.J. Baerends, G. Ricciardi, A. Rosa, S.J.A. van Gisbergen, Coord. Chem. Rev. 230 (2002) 5.
[50] M.J. Root, B.P. Sullivan, T.J. Meyer, E. Deutsch, Inorg. Chem. 24 (1985) 2731.
[51] E.A. Seddon, K.R. Seddon, The Chemistry of Ruthenium, Pergamon, Oxford, 1984.
[52] R. Prasad, Polyhedron 14 (1995) 2151.
[53] R. Ziessel, M. Hissler, A. El-ghayoury, A. Harriman, Coord. Chem. Rev. 178 (1998) 1251.
[54] A. Harriman, M. Hissler, O. Trompette, R. Ziessel, J. Am. Chem. Soc. 121 (1999) 2516.
[55] G.G. Gurzadyan, T.H. Tran-Thi, T. Gustavsson, J. Chem. Phys. 108 (1998) 385.
[56] H. Kano, T. Kobayashi, J. Chem. Phys. 116 (2002) 184.
[57] H.S. Cho, N.W. Song, Y.H. Kim, S.C. Jeoung, S. Hahn, D. Kim, S.K. Kim, N. Yoshida, A. Osuka, J. Phys. Chem. A 104 (2000) 3287.
[58] S. Akimoto, T. Yamazaki, I. Yamazakim, A. Osuka, Chem. Phys. Lett. 309 (1999) 177.
[59] R. Prasad, A. Kumar, Supramol. Chem. 18 (2006) 77.
[60] E.G. Sakellariou, A.G. Montalban, H.G. Meunier, R.B. Ostler, G. Rumbles, A.G.M. Barrett, B.M. Hoffman, J. Photochem. Photobiol. A: Chem. 136 (2000) 185.
[61] H. Kano, T. Kobayashi, Bull. Chem. Soc. Jpn. 75 (2002) 1071.
[62] M. Kasha, J. Chem. Phys. 20 (1952) 71.